

Robotic reactions: Delay-induced patterns in autonomous vehicle systems

Gábor Orosz, Jeff Moehlis, and Francesco Bullo

Department of Mechanical Engineering, University of California, Santa Barbara, California 93106, USA

(Received 9 December 2009; published 22 February 2010)

Fundamental design principles are presented for vehicle systems governed by autonomous cruise control devices. By analyzing the corresponding delay differential equations, it is shown that for *any* car-following model short-wavelength oscillations can appear due to robotic reaction times, and that there are tradeoffs between the time delay and the control gains. The analytical findings are demonstrated on an optimal velocity model using numerical continuation and numerical simulation.

DOI: [10.1103/PhysRevE.81.025204](https://doi.org/10.1103/PhysRevE.81.025204)

PACS number(s): 89.75.Kd, 05.45.-a, 89.40.Bb

I. INTRODUCTION

Early car-following models, such as the California model [1], allowed the study of linear stability of uniform traffic flow. These models already incorporated driver reaction time (see [2] for a review), but at that time the mathematical theory for the corresponding delay differential equations (DDEs) [3] was not available. By the 1990s, nonlinearities penetrated the car-following theory due to the increasing speed and availability of computers, which allowed the exploration of traffic dynamics by means of numerical simulation. The first nonlinear models, such as the optimal velocity model (OVM) [4], were able to reproduce both uniform flow and stop-and-go waves. (In fact, the OVM with reaction-time delay [5] is a nonlinear extension of the California model.) In the last two decades, a large number of car-following models were constructed and investigated by simulations.

Recently, tools from dynamical systems theory have been applied to explore “hidden” unstable motions [6–8] and the effects of reaction-time delay [7–10] in car-following systems. It has been shown that the delay increases the domains of linear instability of the uniform flow. However, drivers may partially compensate for this by anticipatory actions, e.g., by monitoring more than one vehicle in front [9]. On the other hand, sufficiently large excitations (such as sudden braking due to bad lane changes) may still trigger traffic jams even when the uniform flow is linearly stable [7,8,11].

Such excitable dynamics may not allow a traffic engineer to stabilize the uniform flow by controllable message signs. However, one may “substitute” human drivers with autonomous cruise control (ACC) devices that can measure the distances and velocity differences between vehicles by radar, calculate the required action, and actuate cars accordingly [12]. Time delays appear in such systems due to the time needed for sensing, computation, and actuation. Such robotic reaction times are smaller than the human ones, but only the motion of the car immediately in front can be monitored. In [13], ACC dynamics were studied by numerical simulation for a specific model, and short-wavelength oscillations, previously observed in experiments, were detected for certain combinations of gain parameters. The goal of this Rapid Communication is to unveil the dynamical principles underlying such phenomena and to determine the parameter regimes for a general car-following model where the uniform flow can be stabilized by ACCs.

II. MODELING AND STABILITY

Assuming identical vehicles, the acceleration of the i th vehicle is given by

$$\dot{v}_i(t) = f(h_i(t - \tau), \dot{h}_i(t - \tau), v_i(t - \tau)), \quad (1)$$

where the dot stands for differentiation with respect to time t , v_i is the velocity of the i th vehicle, h_i is the distance between the i th and the $i+1$ st vehicles, called the headway, and τ is the reaction-time delay. The system is completed by the kinematic condition

$$\dot{h}_i(t) = v_{i+1}(t) - v_i(t). \quad (2)$$

We assume that system (1,2) possesses a one-parameter set of uniform flow equilibria,

$$h_i(t) \equiv h^*, \quad \dot{h}_i(t) \equiv 0, \quad v_i(t) \equiv v^*, \quad (3)$$

and that there exists a functional relation between the equilibrium headway h^* and the equilibrium velocity v^* ,

$$0 = f(h^*, 0, v^*) \Rightarrow v^* = V(h^*). \quad (4)$$

Here the monotonically increasing non-negative function V expresses that the more sparse traffic is, the faster drivers want to go.

For simplicity, we assume periodic boundary conditions: N vehicles are placed on a circular road of length L , which yields the algebraic equation $\sum_{i=1}^N h_i(t) = L$. This determines the equilibrium headway $h^* = L/N$ and the equilibrium velocity v^* through Eq. (4). We remark that when considering the case of a semi-infinite road, the velocity v^* is prescribed (by the velocity of the leader), and the equilibrium headway is given by $h^* = V^{-1}(v^*)$. In this Rapid Communication, the analytical results are calculated for arbitrary N while the stability charts and bifurcation diagrams are shown for $N=33$. This is small enough to keep the illustrations readable but is large enough to represent the “large N case”: $N \rightarrow \infty$ such that L/N is kept constant. For physically realistic models, the derivatives of f satisfy

$$F = \frac{\partial}{\partial h} f(h^*, 0, v^*) \geq 0, \quad G = \frac{\partial}{\partial h} f(h^*, 0, v^*) \geq 0,$$

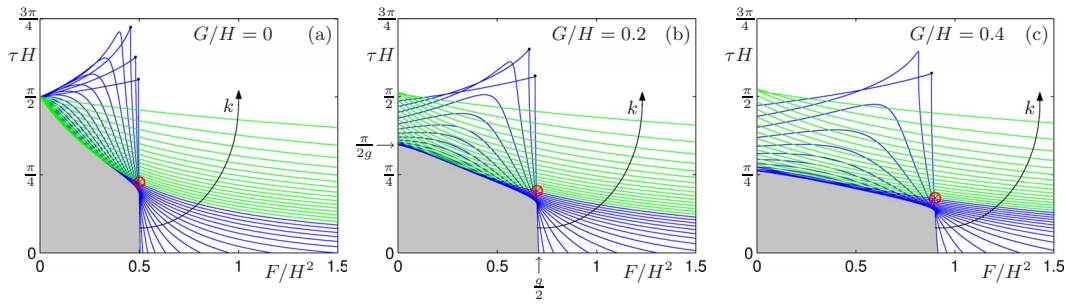


FIG. 1. (Color online) Linear stability diagrams for the general model (1,2). The stable regions are shaded and solid arrows show the increase of the discrete wave number k . For small delay the stability boundary is the $k=1$ curve, while, for larger delay, curves for $k \approx N/2$ constitute the boundary. The red circles locate where the $k=1$ and $k=N/2$ curves intersect. In panel (b), we use the notation $g = 2\frac{G}{H} + 1$.

$$H = -\frac{\partial}{\partial v} f(h^*, 0, v^*) \geq 0, \quad (5)$$

see [11]. (Notice the minus sign in the definition of H .)

When the uniform flow equilibrium (3) loses stability, different spatial patterns may appear. By linearizing the system (1,2) about the uniform flow and using trial solutions proportional to $e^{\lambda t}$, $\lambda \in \mathbb{C}$, one may obtain the characteristic equation. Then considering the critical eigenvalues $\lambda = \pm i\omega$, $\omega > 0$, separating the real and imaginary parts, and using some trigonometric identities, one can determine the Hopf stability curves

$$\frac{F}{H^2} = \frac{\omega}{H} \left[\cos\left(\frac{k\pi}{N}\right) \pm P \right] / \left[2 \sin\left(\frac{k\pi}{N}\right) \right],$$

$$\tau H = \frac{H}{\omega} \arccos \left\{ \frac{H}{\omega} \sin\left(\frac{k\pi}{N}\right) \left[\left(2\frac{G}{H} + 1\right) \cos\left(\frac{k\pi}{N}\right) \pm P \right] \right\},$$

where $P = \sqrt{\frac{\omega^2}{H^2} - \left(2\frac{G}{H} + 1\right)^2 \sin^2\left(\frac{k\pi}{N}\right)}$, (6)

and $k=1, \dots, N-1$ is a discrete wave number. Formula (6) describes stability curves in the $(F/H^2, \tau H)$ plane that are parameterized by the rescaled frequency ω/H , as shown in Fig. 1 for different values of G/H . The uniform flow is stable in the shaded domains, solid arrows indicate the increase of the wave number from 1 to $N-1$, and the curves are colored blue (dark gray) for $k < N/2$ and green (light gray) for $k > N/2$. Since the number of vehicles $N=33$ is odd there is no $k=N/2$ curve; for even N this is located between the “last” blue (dark gray) and the “first” green (light gray) curves. Note that no steady-state bifurcation occurs here, as can be shown by substituting $\lambda=0$ into the characteristic equation.

When crossing a stability curve a Hopf bifurcation takes place; i.e., a pair of complex-conjugate eigenvalues crosses the imaginary axis. In the vicinity of the bifurcation point, the resulting small-amplitude oscillations are traveling waves that can be written in the form $v_i(t) = v^* + v_{\text{amp}} \cos\left(\frac{2k\pi}{N} i + \omega t\right) = v^* + v_{\text{amp}} \cos\left(\pm \frac{2\pi}{\Lambda_{\pm}} s + \omega t\right)$; see [7,11]. Here $s = \frac{L}{N} i$ and the spatial wavelength is $\Lambda_+ = \frac{L}{k}$ for $k \leq N/2$ and $\Lambda_- = \frac{L}{N-k}$ for $k > N/2$; i.e., the same spatial pattern arises for wave numbers k and $N-k$.

Figure 1 shows that for small delay the curve for the lowest wave number $k=1$ is the stability boundary, while for larger delay the $k \approx N/2$ curves constitute the boundary. This means that when increasing F for small delay, the uniform flow loses stability to long-wavelength oscillations and waves of shorter and shorter wavelengths show up when further curves are crossed. For sufficiently large delay, however, short-wavelength oscillations appear first and these are followed by waves of longer wavelengths. That is, the time delay can qualitatively alter the spatial dynamics for ACC systems.

In order to explain this qualitative change, we focus our attention to what happens along the horizontal and vertical axes. For $\tau=0$ (along the horizontal axis in Fig. 1), one may eliminate the frequency ω from Eq. (6) and obtain

$$\frac{F}{H^2} = \frac{1}{2} \left(2\frac{G}{H} + 1\right) \left[\left(2\frac{G}{H} + 1\right) \tan^2\left(\frac{k\pi}{N}\right) + 1 \right], \quad (7)$$

which increases as k grows from 1 toward $N/2$. (Note that the $k > N/2$ curves do not cross the horizontal axis.) This result agrees with the proof constructed in [11] for the non-delayed system. Similarly, for $F=0$ (along the vertical axis in Fig. 1), eliminating ω yields

$$\tau H = \frac{\arctan \left\{ \left[\left(2\frac{G}{H} + 1\right) \tan\left(\frac{k\pi}{N}\right) \right]^{-1} \right\} + \frac{k\pi}{N}}{\sqrt{1 + 4\frac{G}{H} \left(\frac{G}{H} + 1\right) \sin^2\left(\frac{k\pi}{N}\right)}}, \quad (8)$$

which reaches its minimum when $k \approx N/2$. The change in the order of curves along the axes makes it necessary that curves for different wave numbers cross each other in the $(F/H^2, \tau H)$ plane. These crossings correspond to codimension-two Hopf bifurcations that potentially lead to complex dynamics. (A curve may cross itself as occurs at the points denoted by black dots in Fig. 1.)

To approximate the value of the delay where qualitative change occurs (i.e., locate the small region in the middle of the panels where most curves cross each other) we calculate where the $k=1$ and the $k=N/2$ curves intersect (in the large

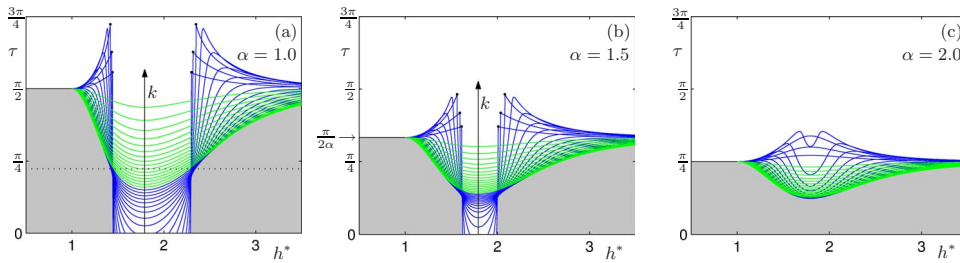


FIG. 2. (Color online) Linear stability diagrams for the OVM (1,2,12,13) corresponding to Fig. 1(a), i.e., for $G=0$. Notation as in Fig. 1 and the horizontal dotted line in panel (a) corresponds to the bifurcation diagrams in Figs. 3(a) and 3(b).

N limit). These points are highlighted by the red circles in Fig. 1. First, notice that in the vicinity of the intersection the $k=1$ curve is well approximated by a vertical line located at

$$\frac{F}{H^2} = \frac{1}{2} \left(2 \frac{G}{H} + 1 \right) := \frac{1}{2} g, \quad (9)$$

that is obtained by considering $\tau=0$ and $k/N \rightarrow 0$. Indeed, $G \geq 0 \Leftrightarrow g \geq 1$. Substituting Eq. (9) and $k=N/2$ into Eq. (6) and eliminating ω , one obtains

$$\begin{aligned} \tau H &= \frac{1}{g} \sqrt{\frac{2}{1 + \sqrt{1 + 4g^{-2}}}} \arccos \left[\frac{1}{g} \frac{2}{1 + \sqrt{1 + 4g^{-2}}} \right] \\ &\geq \frac{\pi/2}{g + \pi/2}, \end{aligned} \quad (10)$$

where the larger g is, the better the lower estimation is. For $G=0 \Leftrightarrow g=1$ [Fig. 1(a)], Eq. (10) simplifies to

$$\tau H = \sqrt{\frac{1}{\varphi}} \arccos \left[\frac{1}{\varphi} \right] \approx 0.711, \quad (11)$$

where $\varphi = (1 + \sqrt{5})/2 \approx 1.618$ is the golden ratio.

One may observe a tradeoff in the stability charts in Fig. 1: when G is increased, there is an increase of stability in F but a decrease of stability in τ , that is, the stable domain is stretched in one direction but squeezed in the other. Similar deformation occurs when H is increased as will be explained below on a concrete example. This means that a common rule of thumb of the nondelayed system, namely that increasing the gains G and H is beneficial for stability, is violated when the delay is sufficiently large.

III. OPTIMAL VELOCITY MODEL

Formula (1) with restriction (5) on the signs of derivatives describes a large family of nonlinear models. Here we demonstrate the above linear results and their possible consequences for the nonlinear dynamics on a concrete nonlinear car-following model, the OVM [4,5,7,8] where

$$f(h, \dot{h}, v) = \alpha [V(h) - v], \quad (12)$$

and the V determines the equilibrium according to (4). Here we use the dimensionless function

$$V(h) = \begin{cases} 0, & \text{if } h \in [0, 1] \\ \frac{(h-1)^3}{1 + (h-1)^3}, & \text{if } h \in [1, \infty) \end{cases}, \quad (13)$$

where space is rescaled by the stopping distance (below which $V(h) \equiv 0$) and velocity is rescaled by the maximum velocity (that is approached when $h \rightarrow \infty$); see [8].

Knowing f explicitly allows us to transform the stability charts to physically meaningful parameters (such as the average headway $h^* = L/N$). The derivatives in Eq. (5) become

$$F = \alpha V'(h^*), \quad G = 0, \quad H = \alpha, \quad (14)$$

and using (6,13,14) one may draw stability charts in the (h^*, τ) plane for different values of α , as depicted in Fig. 2. These correspond to the chart in Fig. 1(a) with $\tau H = \tau \alpha$ and $F/H^2 = V'(h^*)/\alpha$. For small α there are two “copies” of the stable domain on the left and the right sides, while for larger α these areas merge. Indeed, when varying h^* for sufficiently large delay, the “first” instability yields short-wavelength oscillations. A tradeoff can also be observed: when α is increased the width of the unstable domain decreases (and even disappears for small delay) but the height of the stable domain decreases. One may show that there is a critical delay ($\tau_{\text{crit}} \approx 0.39$) above which the unstable domain cannot be diminished by increasing the gain parameter α . We remark that for $h^* \leq 1$ the model (1,2,12,13) simplifies to $\dot{v}_i(t) = -\alpha v_i(t - \tau)$, $i = 1, \dots, N$. This is a classic example of a linear scalar delay differential equation [3] that is stable for $\tau < \frac{\pi}{2\alpha}$ as pointed out in Fig. 2(b).

We use numerical continuation techniques [14] to demonstrate the complexity that can arise at the nonlinear level due to the change in the order of stability curves. These techniques allow us to trace both stable and unstable oscillatory solutions (traveling waves) arising from the Hopf bifurcation points. We fix $\alpha = 1.0$ and $\tau = 0.7$, that is, we study the system along the dotted horizontal line in Fig. 2(a). In Fig. 3(a) the amplitude of velocity oscillations is shown for different wave numbers, with detail of the top of the branches in Fig. 3(b). Stable and unstable states are represented by green (light gray) and red (dark gray) curves, respectively. The horizontal axis represents the uniform flow and Hopf bifurcations are denoted by blue stars along the axis. The outermost bifurcations are subcritical, so unstable oscillations/waves appear “before” the uniform flow loses stability.

The branches of oscillations undergo further bifurcations. Fold bifurcations (denoted by blue crosses) occur where branches fold back, while Neimark-Sacker and period-doubling bifurcations (denoted by blue stars and blue diamonds) happen where the stability changes. In the latter cases, quasiperiodic oscillations arise that are not studied in detail in this Rapid Communication. We recall that without delay the only stable oscillatory solution is the one-wave solution [6] and this feature is preserved for small delays.

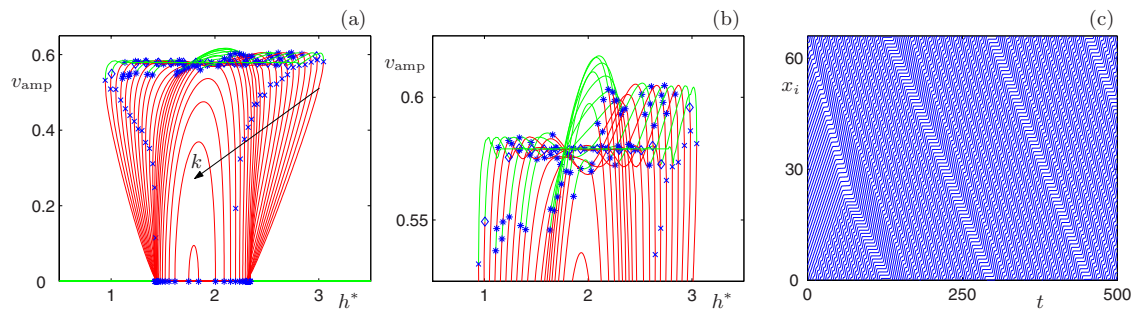


FIG. 3. (Color online) In panel (a) the amplitude of velocity oscillations is shown for different wave numbers for the OVM (1,2,12,13) and a zoom of the top section is displayed in panel (b). Stable and unstable solutions are shown as green (light gray) and red (dark gray) curves, respectively. The solid arrows represent the increase of the wave number k for large amplitude. Panel (c) shows a spatiotemporal plot generated by an initial value simulation at $h^*=2.0$.

However, our results indicate that, for sufficiently large delay, oscillations for larger wave numbers (shorter wavelengths) may also become stable. Notice that even though the order of wave numbers is nonincreasing along the horizontal axis, the increasing order is gained back for larger amplitude, as shown by the solid arrow in Fig. 3(a).

To visualize the resulting spatial patterns we use numerical simulations. The spatiotemporal plot in Fig. 3(c) is shown for $\alpha=1.0$, $\tau=0.7$, $h^*=2.0$ that corresponds to the middle of Figs. 3(a) and 3(b). [The constraint $v_i(t) \geq 0$, $i=1, \dots, N$ is used to eliminate unphysical motions such as reversing.] The initial conditions are chosen to be constant functions along the interval $[-\tau, 0]$ such that vehicles are placed into the uniform flow equilibrium except one whose velocity and headway is reduced to mimic the effect of a sudden braking. The effect of braking propagates against the flow leading to a long-wavelength stop-and-go wave. Simultaneously, short-wavelength oscillations develop “spontaneously”; i.e., a state that is a “mixture” of long- and short-wavelength motions is approached. As time progresses the long-wavelength regime becomes narrower and this would occur faster if noise was added to the system. The detailed analysis of such patterns will be the subject of future research.

IV. DISCUSSION

ACCs are primarily developed to increase the drivers’ comfort for individual vehicles, but, as was shown above, these devices may also help to avoid congestion. To achieve this goal it is essential to take into account the above design principles (delay-induced short-wavelength instabilities and delay-gain tradeoffs) when designing ACC algorithms. The digital controllers built into the robotic vehicles sample time periodically and hold the accelerations constant during the sampling period [15]. Exploring the effects of such quantization is an interesting future research direction. Finally, even though ACCs are only capable of controlling the one-dimensional (longitudinal) motion of cooperative vehicles systems, one may expect that time delays become important for two-dimensional vehicle configurations, especially for high-speed maneuvers [16,17].

ACKNOWLEDGMENTS

G.O. acknowledges discussions with Arne Kesting, Gábor Stépán, Jonathan Ward, and Eddie Wilson. This research was supported by the Institute for Collaborative Biotechnologies under Grant No. DAAD19-03-D004 from the U.S. Army Research Office.

-
- [1] R. E. Chandler, R. Herman, and E. W. Montroll, *Oper. Res.* **6**, 165 (1958).
 [2] E. N. Holland, *Transp. Res., Part B: Methodol.* **32**, 141 (1998).
 [3] G. Stépán, *Retarded Dynamical Systems* (Longman, London, 1989).
 [4] M. Bando, K. Hasebe, A. Nakayama, A. Shibata, and Y. Sugiyama, *Phys. Rev. E* **51**, 1035 (1995).
 [5] M. Bando, K. Hasebe, K. Nakanishi, and A. Nakayama, *Phys. Rev. E* **58**, 5429 (1998).
 [6] I. Gasser, G. Siritto, and B. Werner, *Physica D* **197**, 222 (2004).
 [7] G. Orosz and G. Stépán, *Proc. R. Soc. London, Ser. A* **462**, 2643 (2006).
 [8] G. Orosz, R. E. Wilson, R. Szalai, and G. Stépán, *Phys. Rev. E* **80**, 046205 (2009).
 [9] M. Treiber, A. Kesting, and D. Helbing, *Physica A* **360**, 71 (2006).
 [10] W. Michiels, C.-I. Morărescu, and S.-I. Niculescu, *SIAM J. Control Optim.* **48**, 77 (2009).
 [11] R. E. Wilson, *Philos. Trans. R. Soc. London, Ser. A* **366**, 2017 (2008).
 [12] A. Kesting, M. Treiber, M. Schönhof, and D. Helbing, *Transp. Res., Part C: Emerg. Technol.* **16**, 668 (2008).
 [13] A. Kesting and M. Treiber, *Comput. Aided Civ. Infrastruct. Eng.* **23**, 125 (2008).
 [14] D. Roose and R. Szalai, in *Numerical Continuation Methods for Dynamical Systems*, edited by B. Krauskopf, H. M. Osinga, and J. Galan-Vioque (Springer, New York, 2007), pp. 359–399.
 [15] G. Stépán, *Int. J. Solids Struct.* **38**, 2149 (2001).
 [16] R. M. Murray, *J. Dyn. Syst., Meas., Control* **129**, 571 (2007).
 [17] F. Bullo, J. Cortés, and S. Martínez, *Distributed Control of Robotic Networks* (Princeton University Press, Princeton, NJ, 2009).